# Molecular-dynamics subplantation studies of carbon beneath the diamond (111) surface

Sylke Uhlmann, Thomas Frauenheim, and Uwe Stephan
*Technische Universität, Institut für Physik, Theoretische Physik III, Postfach 964, D-09009 Chemnitz, Germany*
(Received 30 August 1994; revised manuscript received 24 October 1994)

The near-surface implantation of hyperthermal neutral carbon atoms of energy 15–75 eV onto a low-temperature diamond (111) substrate is studied by molecular dynamics using a density-functional-based nonorthogonal tight-binding scheme. Depending on the initial energy and the impact point, the atoms penetrate beneath the exposed (111) surface forming regions of local disorder and stress. The energy partition during the collision is analyzed, yielding results about penetration and the displacement threshold. After a final relaxation of the structures we determine the penetration depth of the colliding particles. The structural topology and the electronic properties of the induced defects and surface modifications are discussed.

## I. INTRODUCTION

Within the past decade there has been a growing interest in a fundamental understanding of low-temperature, low-pressure synthesis of diamond films[1] using low-energy ion beams directed towards low-temperature crystalline substrates. By applying various experimental techniques[2–5] and theoretical simulations,[6–11] valuable data on the bonding states, structure, saturation, and electronic properties of as-grown diamond films have been obtained. However, to understand and finally to control the film growth under low-energy ion-beam conditions there are only very few attempts in theoretical simulations on how the diamond surface would behave under energetic particle impact.[12,13]

In Kaukonen and Nieminen's work[12] the main goal is to study the growth of diamondlike films on a low-temperature diamond substrate by using the *empirical* Tersoff potential.[14] Pailthorpe[13] focuses more directly on the behavior of the diamond surface during collision. He performed interesting classical molecular-dynamics (MD) simulations of 1–100 eV neutral carbon atom collisions with a clean unreconstructed low-temperature diamond (111) surface using an empirical Stillinger-Weber potential with a reparametrization derived from Hartree-Fock calculations for small tetrahedral carbon clusters. Pailthorpe showed that carbon atoms with energies between 20 and 60 eV are able to penetrate the surface forming regions of increased stress which favor quaternary coordination. However, the interatomic potential used is fixed for $sp^3$ bonding configurations. This is reliable only for the early stages of near-surface interactions of incoming particles having higher energies than typical bond energies. In order to realistically describe the surface near relaxation, defect creation, and reconstruction during the slackening of the projectile it is essential to use *first-principles*-based methods which properly describe the various carbon hybridization states rather than empirical potentials fitted to equilibrium configurations.

In Sec. II we outline a simple, efficient, and sufficiently accurate density-functional (DF) based tight-binding (TB) method for a realistic calculation of interatomic forces from total structural energies as a function of the coordinates of all atoms at the structure. After that, in Sec. III we describe the collision geometry and the regime for modeling effects in low-energy ion collisions onto a crystalline diamond substrate. The main results on the penetration behavior of neutral carbon atoms into diamond and the classification of generated defects are discussed in Sec. IV, before summarizing in Sec. V.

## II. DF MD METHOD

Within the Born-Oppenheimer approximation, the interatomic forces for the MD simulations of neutral carbon atom collisions onto the diamond (111) surface are calculated on the basis of a DF-related nonorthogonal TB approach.

In the framework of the linear combination of atomic orbitals (LCAO) formalism we use the local-density approximation (LDA) for a self-consistent calculation of suitable input charge densities and atomic potentials. The Kohn-Sham wave functions of the many-atom structure are expanded as a LCAO ansatz with respect to a minimal basis of all valence electron orbitals centered at the atomic nuclei. In this way the Kohn-Sham equations transform into a set of algebraic equations for the determination of the single-particle electronic eigenenergies and wave functions. By only considering two-center integrals the Hamiltonian and overlap matrix elements are calculated directly out of the local orbital basis and atomic potentials rather than fitted to experimental data as usually done in parametrized TB schemes. The Hamiltonian and overlap integrals are calculated once for all the time in dependence on the interatomic separation, which makes this scheme very efficient for any application in molecular dynamics.

After solving a general eigenvalue problem for determining the occupied single-particle energies and eigen-

 

functions, the cohesive energy of the structure now in a common way can be written as a sum of two parts

$$E_{\rm tot}(\{\mathbf{R}_l\}) = E_{\rm bind}(\{\mathbf{R}_l\}) + E_{\rm rep}(\{\mathbf{R}_l - \mathbf{R}_k\}) = \sum_i n_i \varepsilon_i(\{\mathbf{R}_l\}) + \sum_l \sum_{<k} V_{\rm rep}(\{\mathbf{R}_l - \mathbf{R}_k\}).$$

The first part includes the electronic binding contributions as a sum over all occupied single-particle energies $\varepsilon_i$ with occupation number $n_i$ and the second, as a repulsive energy, is modeled by short-range two-particle potentials that still need fitting to self-consistent cohesive energy calculations performed on the LDA level.[15] The method has proven to be highly transferable to all scale carbon and hydrocarbon systems. The determination of equilibrium geometries, cohesive energies, and vibrational modes of a representative class of microclusters, molecules, and solid state modifications yields results with overall good agreement with more sophisticated methods.[15,16] As a further example, the activation barrier for the concerted exchange of two atoms using a minimum energy path[17] obtained by our method equals 19.5 eV. This value should be compared to 13.2 eV, as found by self-consistent field (SCF) LDA calculations based on nonlocal soft pseudopotentials and the plane-wave method.[18] Recently the described method has been successfully applied to investigations of structure formation in amorphous carbon modifications[11,19,20] and on diamond surfaces as well.[21,22]

The interatomic forces can easily be calculated from the gradients of the total energy at all atom sites:

$$\begin{aligned}\mathbf{F}_l = M_l \ddot{\mathbf{R}}_l &= -\frac{\partial E_{\rm tot}(\{\mathbf{R}_l\})}{\partial \mathbf{R}_l} \\ &= -\frac{\partial(\psi_i|\hat{h}|\psi_i)}{\partial \mathbf{R}_l} \\ &= \sum_i n_i \sum_\mu \sum_\nu c_\mu^i c_\nu^i \left[-\frac{\partial h_{\mu\nu}}{\partial \mathbf{R}_l} + \varepsilon_i \frac{\partial S_{\mu\nu}}{\partial \mathbf{R}_l}\right] \\ &\quad -\frac{\partial E_{\rm rep}}{\partial \mathbf{R}_l}.\end{aligned} \tag{1}$$

The applied MD scheme may be viewed as a hybrid between *full-potential* SCF molecular dynamics[23,24] and the use of classical *empirical* potentials[14,25,26] or *empirical* orthogonal tight-binding schemes.[27] The method is almost as simple to use as parametrized nonorthogonal tight-binding schemes,[28] and this with an accuracy and transferability being close to SCF calculations.

## III. COLLISION GEOMETRY AND SIMULATION REGIME

All computational experiments have been performed by using a two-dimensional periodic thin-slab supercell geometry of diamond with a (111) surface saturated by hydrogen. In order to optimize the computational time, the thickness of the film has been varied between 8 and 16 carbon layers corresponding to the initial energy of the projectile. Each layer of the initial slab contained 12 atoms. The carbon atoms of the two bottom layers have been fixed at their crystalline positions to simulate an infinite substrate. Before each collision the initial temperature of the slab has been set to 0 K. The impinging carbon atoms enter the surface normally with varying the initial energy between 15 and 75 eV. The investigation of higher impact energies requires a more extended supercell model because of interactions with neighboring supercells as well as collision cascades moving below the bottom layer of the slab. To solve Newton's equations of motion by the Verlet algorithm, different discrete time scales in the scattering and relaxation regime have to be applied. Whereas during the collision of the incoming particle a time step width of 5 atu (1 atu= $2.4\times10^{-17}$ s) has proven to be short enough, the final relaxation has been performed at 20 atu. Taking into account the still considerable computational effort, it has not been possible yet to analyze a wide range of impact points and to perform a statistical sampling of all events. Therefore, five different impact points were chosen on the surface of the film: the centers of a first-layer atom; a second-layer atom, and a fourth-layer atom; the center of a bond between a first- and second-layer atom; and, finally, a direction normally into a void. Clearly, there are different probabilities for these impact points to occur in real systems, but they allow us to define an area of possible reactions and processes.

As mentioned before, the simulation has to be split into two successive regimes of different time scales: a collisional phase and a relaxation phase. During the collision the slab is strongly heated up from a thermal spike. Comparing the time for the energy transfer in the collision cascade slackening, the impact particle (about $10^{-14}$ s), and the time necessary for local thermal equilibration (about $10^{-8}$ s), there is obviously a difference in orders of magnitude. This cannot be handled properly by applying our MD scheme. Therefore, as an approximate modeling of the collison in the first phase, the slab is thermally isolated within an interval of 2000 atu which correlates with a degree of energy dissipation excluding further displacements. In this way, the total amount of impact energy is transferred into displacements and lattice heating. Within these processes highly nonequlibrium configurations are generated that have to be relaxed within a second simulation regime. The heated structures are relaxed in three steps: a starting equilibration, a cooling down sequence, and a final equilibration. The velocities of all atoms are scaled with respect to a temperature-time function after a random number of time steps. The temperature-time dependence consists of three intervals according to the three annealing steps: there are two intervals of constant temperature for starting a final equilibration and an exponential fit between starting and final temperature.[29] The time used for the equilibration run is 4000, 50.000, and 4000 atu (approximately 1.4 ps), respectively. For an estimation of the starting temperature of the relaxation regime, all atoms with velocities higher than 90% of the maximum velocity have been excluded. An assessment of this treatment is achieved by a comparison of the total energies of the final collisional structure and the structure after the first equilibration steps at the estimated temperature.

## IV. RESULTS AND DISCUSSION

One main topic of interest in low-energy ion collisions is the investigation of energy partition and dissipation during surface penetration. In Fig. 1(a) the initial maximum penetration and in Fig. 1(b)the final resting positions of the impact particles after relaxation for all impact points versus initial energy are shown.

There is a very sensitive dependence of the penetration behavior on the scattering parameter. The tendency of increasing initial penetration with increasing impact energy is the same for all scattering parameters. However, the absolute depth varies with the chosen impact point and hence the amount of energy lost during the interaction with the nearest first-layer atoms. At the smallest considered energies of 15 eV the incoming atom hardly penetrates the surface as already discussed by Pailthorpe.[13] Whereas in first- and second-layer collisions the subsurface is locally heated and the incoming atoms are backscattered desorbing hydrogen from the surface, the central to bond and fourth layer directed atoms already have high enough energy to form stable interstitials within the top surface layer after relaxation. Relaxing the first- and second-layer scattering events the CH radical finally traps the dangling bond site. Increasing the energy, only in the central to void collisions, the depth increases linearly, indicating a channelinglike behavior on a minimum energy path through the structure of the top layers. The initial kinetic energy dissipates into lattice heating in a continuous and relatively isotropic manner. The lattice relaxation effects in this case are minimal and the final resting positions almost match the initial maximum penetration. So, atoms with an initial energy of 75 eV impinging into a void or central to a fourth-layer atom reach a maximum depth of $8.5a_0$ ($a_0$ denotes the Bohr radius), which is much deeper than the value reported from the scattering events of Pailthorpe.[13] For a comparison the depth of the final resting positions after relaxing the structures are shown in Fig. 1(b).

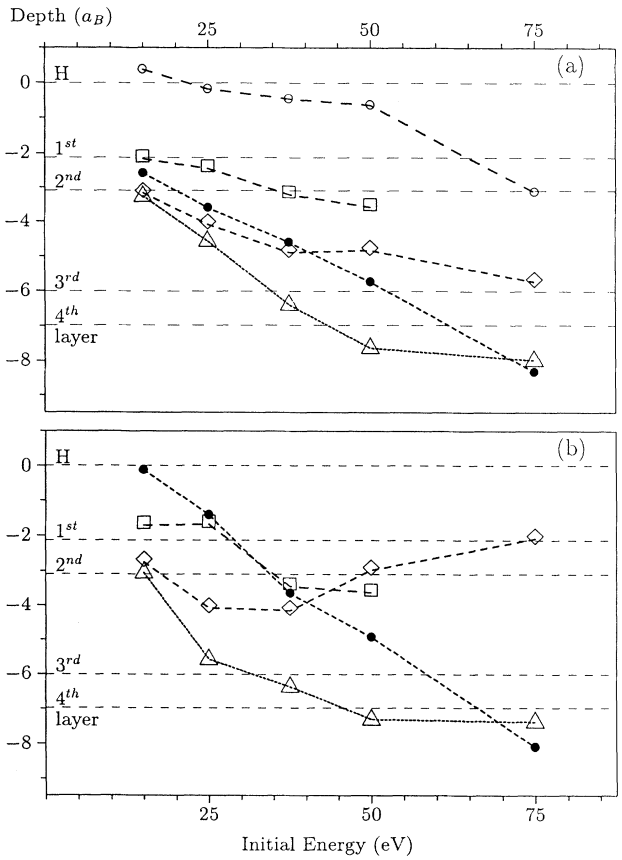


FIG. 1. Maximum (a) and final (b) penetration depth of projectiles in dependence on the initial energy for different impact points: ◇, to the center of a bond; ○, central to a first-layer atom; □, central to a second-layer atom; △, central to a fourth-layer atom; •, into a void.

Following the trajectories of the bond-directed projectile with increasing energy the largest surface layer distortions are observed during penetration. The impact particle induces high lateral stress that is lowered by lattice relaxation, resulting in a five- and seven-membered ring structure at 50-eV impact energy. The strong surface layer relaxation is also confirmed by a considerable reduction of the final penetration depth in the case of the bond-directed projectiles in Fig. 1(b).

In the other extreme of central to surface (first and second layer) atom collisions the energy and the momentum due to the equal mass of the target atoms are almost ideally exchanged. This process may either displace a surface atom to a deeper crystal layer if the energy exceeds some critical value or the incoming particle again is reflected, leaving a local heat spot if its energy is too low. Atoms hitting centrally on a first-layer atom all leave the surface with a bonded hydrogen. At an initial energy of 15 eV, after relaxation, the CH radical saturates the dangling bond of the former hydrogen site, and for initial energies of 50 and 75 eV the generated vacancy in the surface layer (resulting from displacing the first-layer atom) is filled by the projectile. That is why the final positions of first-layer projectiles are not shown in Fig. 1(b).

Interesting results are obtained by analyzing the second- and fourth-layer impact processes. There are clear discontinuities of the final positions between 25 and 40 eV in the former and between 50 and 75 eV in the latter case, indicating displacement thresholds in the observed energy ranges. Obviously, the central energy transfer to any target atom down to the fourth layer at 75 eV is high enough to remove it from its original lattice site and to induce a displacement cascade.

As a quantitative result the minimum displacement threshold for a (111) surface has been determined by monitoring the first-layer atom impact scattering processes versus time. Figure 2 shows the motion of the first-layer target atom during the collision for several initial projectile energies in the range of interest. Whereas at all energies below 28 eV only vibrations of the atom around its equilibrium position with growing amplitude and period were observed, the target atom at 28 eV and higher initial energies is displaced irreversibly to a deeper crystal layer. This serves as an indication of a sharp

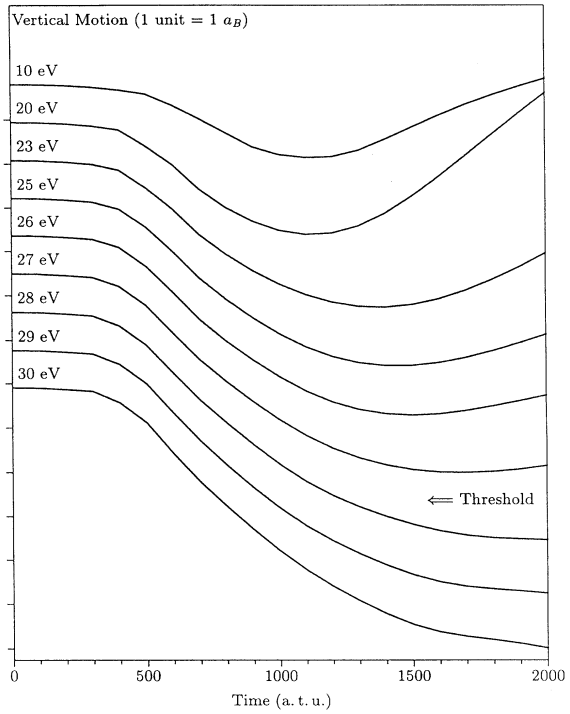


FIG. 2. Vertical motion of the first-layer impact target atom versus time for different initial energies in the range of the displacement threshold.

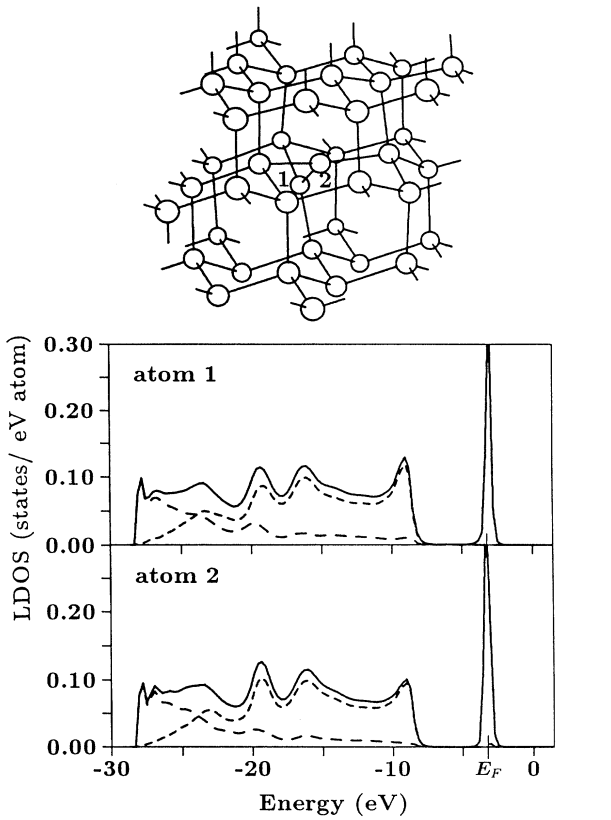


FIG. 3. Local densities of states of a ⟨100⟩ split within the third double layer (2), caused by a 50-eV atom impact central to a first-layer atom. The bonding geometry of the defect environment is shown in the upper part of the figure (open circles, carbon atoms; filled circles, hydrogen atoms). The partial LDOS of $s$ and $p$ electrons are plotted as long and short dashed lines, respectively.

displacement threshold. Because of the central impact, the amount of energy transferred to the target atom attains a maximum, while the lattice relaxation is minimized since no other atom is situated in the neighborhood in the normal direction. Furthermore, the first-layer atom has only three bonds to other carbon atoms in comparison to the fourfold bonded bulk atoms. Consequently, the estimated energy value is a theoretically proposed lower bound of the surface atom displacement threshold for low-energy C-atom collisions in the [111] impact direction. Taking into account that it is hard to generate monoenergetic carbon beams, this value cannot be confirmed experimentally up to now. Experiments have been performed by energetic electron beams measuring a threshold energy of (47.6 ± 1.3) eV in the [111] direction.[30] This value may be compared to a 37.5-eV displacement threshold for a central to second-layer collision in Fig. 1(b). Considering that the energy and momentum transfer with very-low-mass electrons is not ideal, the theoretical bound for this displacement with a carbon atom is very reasonable.

To picture the influence on the electronic structure the local densities of states (LDOS) for several defect atoms have been calculated;[11,30,31] cf. Figs. 3–5. The depths where these defect configurations occur depend on the initial energies and the impact parameters. The final configurations of the point defects after relaxation in Figs. 3 and 4 can be described by a local structure according to a ⟨100⟩ split interstitial.[18] The defect in Fig. 3 resides in the third double layer. It accrued by impact of a 50-eV carbon atom directed to a first-layer atom and consists of cascade atoms. The threefold coordinated defect pair is embedded within the $sp^3$ matrix. The noninteracting $p$ states of these two defect atoms produce two degenerate states at the Fermi energy. The second defect in Fig. 4 within the first double layer is generated by a carbon atom hitting centrally a bond between two surface atoms at an initial energy of 75 eV. The two defect atoms 1 and 2 as well as the neighboring first-layer atom 3 are threefold coordinated, the latter having a dangling bond because of the loss of a hydrogen atom. The LDOS of the two first-layer atoms show two $\pi$-$\pi^*$ states in the gap according to a $\pi$ bond between these atoms. The third state near the Fermi energy arises due to the dangling bond of the deeper-lying defect atom.

In Fig. 5 the LDOS of a more extended near-surface defect is shown. This structure has arisen from the impact of a carbon atom with an initial energy of 50 eV directed centrally to a bond. As the result, one hydrogen atom has been replaced by a carbon atom that was removed from its lattice site by the projectile. Additionally, the positions of two fourfold coordinated atoms 3

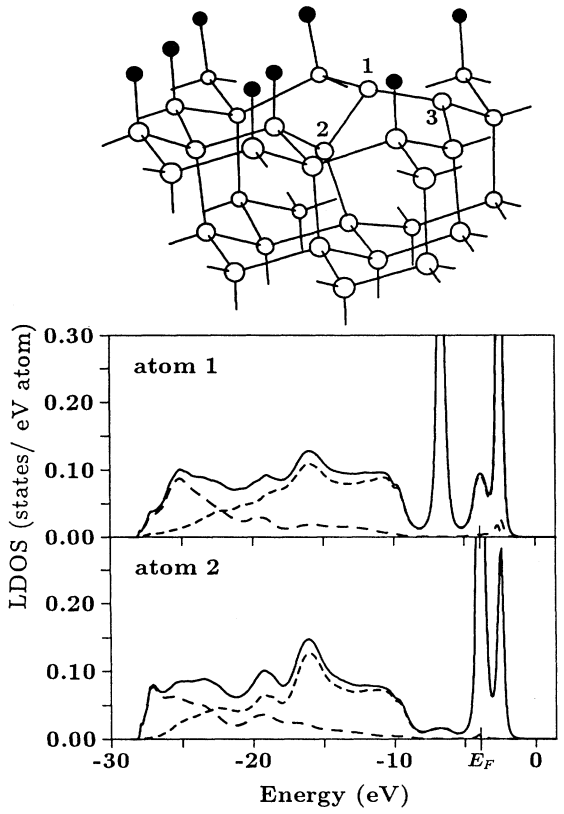


FIG. 4. Local densities of states of a two-atomic defect within the first double layer similiar to a strained ⟨100⟩ split. The bonding geometry of the defect environment is shown in the upper part of the figure (open circles, carbon atoms; filled circles, hydrogen atoms). The partial LDOS of $s$ and $p$ electrons are plotted as long and short dashed lines, respectively.

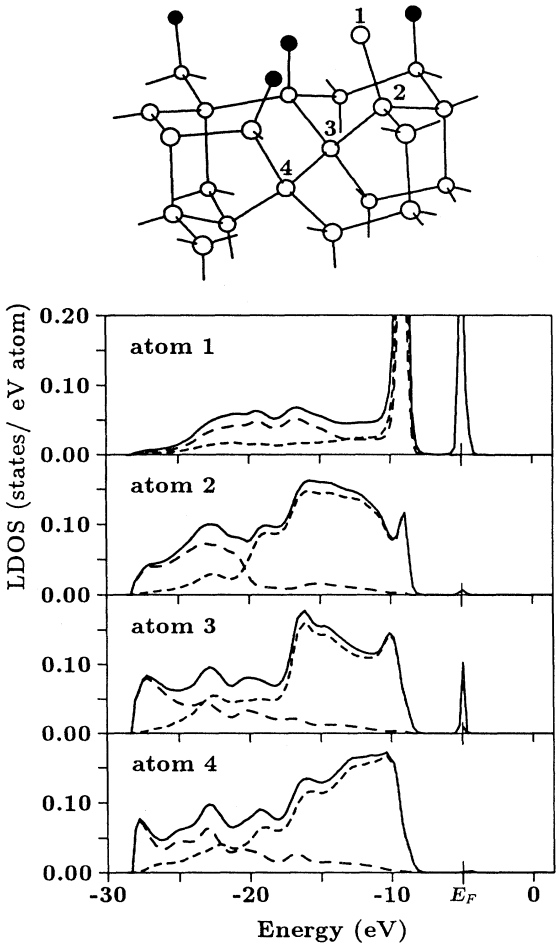


FIG. 5. Local densities of states of four atoms of a near-surface defect, caused by the impact of a 50-eV projectile (atom 2) directed centrally to a bond between a first- and a second-layer atom. The bonding geometry of the defect environment is shown in the upper part of the figure (open circles, carbon atoms; filled circles, hydrogen atoms). The partial LDOS of $s$ and $p$ electrons are plotted as long and short dashed lines, respectively.

and 4 within the second and third layers were largely distorted. The defect states in the gap are caused by the unsaturated orbitals of atom 1 which produce degenerate nonbonding $p$-like states (with weight 1.8 in the LDOS, related to the total weight 4.0). These states extend over a few next-nearest neighbors starting from atom 1, but fall off rapidly with distance in the fourfold coordinated bulk environment. Therefore, this defect does not produce any pronounced states within the gap of atoms 2 and 4.

## V. SUMMARY

We have performed density-functional-based nonorthogonal tight-binding calculations of subplantation molecular dynamics of carbon atoms onto a (111) diamond surface by using a simplified LDA LCAO scheme to calculate the interatomic forces for atomic motion. In agreement with previous simulations,[13] the effect of the carbon atom collision strongly depends on the initial energy. However, as found in our calculations, the final penetration depth after relaxation is considerably larger than that originally proposed by Pailthorpe.[13] This should be due to the use of a much more flexible interatomic potential in the present investigations derived on a density-functional basis and allowing for all hybridization changes occurring in carbon systems. As a consequence, the diamond surface in the relaxation by using tetrahedrally fixed potentials has to be expected as too rigid. Furthermore, in our results the depth of the final resting positions strongly depends on the chosen impact point. As an important outcome of our calculations we found an estimate of a minimal displacement threshold of 28 eV for first-layer atoms in the [111] direction. The morphologic and electronic structure of the resulting defects have been analyzed.

## ACKNOWLEDGMENT

We gratefully acknowledge support from the Deutsche Forschungsgemeinschaft.

[1] J. C. Angus and C. C. Hayman, Science **241**, 913 (1988).
[2] H.-G. Busmann, H. Sprang, I. V. Hertel, W. Zimmermann-Edling, and H.-J. Güntherodt, Appl. Phys. Lett. **59**, 295 (1991).
[3] H. Sprang, S. Lauer, H.-G. Busmann, and I. V. Hertel, Appl. Phys. A **55**, 347 (1992).
[4] T. Tsuno, T. Imai, Y. Nishivayashi, K. Hamada, and F. Fujimori, Jpn. J. Appl. Phys. **30**, 1063 (1991).
[5] H.-G. Busmann, W. Zimmermann-Edling, H. Sprang, H.-J. Güntherodt, and I. V. Hertel, Diamond Relat. Mater. **1**, 979 (1992).
[6] B. J. Garrison, E. J. Dawnkaski, D. Srivastava, and D. W. Brenner, Science **255**, 835 (1992).
[7] S. Skokov, B. Weiner, and M. Frenklach, J. Chem. Phys. **98**, 7073 (1994).
[8] D. R. Alfonso, D. A. Drabold, and S. E. Ulloa, Phys. Rev. B **51**, 1989 (1995).
[9] S. Iarlori, G. Galli, F. Gigy, M. Parrinello, and E. Tosatti, Phys. Rev. Lett. **69**, 2947 (1992).
[10] S. A. Yang, D. A. Drabold, and J. B. Adams, Phys. Rev. B **48**, 5261 (1993).
[11] Th. Frauenheim, P. Blaudeck, U. Stephan, and G. Jungnickel, Phys. Rev. B **48**, 4823 (1993).
[12] H.-P. Kaukonen and R. M. Nieminen, Phys. Rev. Lett. **68**, 620 (1992).
[13] B. A. Pailthorpe, J. Appl. Phys. **70**, 543 (1991).
[14] J. Tersoff, Phys. Rev. Lett. **56**, 632 (1986); Phys. Rev. B **37**, 6991 (1988); Phys. Rev. Lett. **61**, 2879 (1988).
[15] D. Porezag, Th. Frauenheim, Th. Köhler, G. Seifert, and R. Kaschner (unpublished).
[16] M. T. Yin and M. L. Cohen, Phys. Rev. Lett. **50**, 2006 (1983).
[17] K. C. Pandey, Phys. Rev. Lett. **57**, 2287 (1986).
[18] J. Bernholc, A. Antonelli, and T. M. Del Sole, Phys. Rev. Lett. **61**, 2689 (1988).
[19] U. Stephan, Th. Frauenheim, P. Blaudeck, and G. Jungnickel, Phys. Rev. B **50**, 1048 (1994).
[20] G. Jungnickel, Th. Frauenheim, D. Porezag, P. Blaudeck, U. Stephan, and R. J. Newport, Phys. Rev. B **50**, 6709 (1994).
[21] Th. Frauenheim, U. Stephan, P. Blaudeck, D. Porezag, H.-G. Busmann, W. Zimmermann-Edling, and S. Lauer, Phys. Rev. B **48**, 18189 (1993).
[22] P. Blaudeck, Th. Frauenheim, H.-G. Bussmann, and Th. Lill, Phys. Rev. B **49**, 11409 (1994).
[23] R. Car and M. Parinello, Phys. Rev. Lett. **55**, 2471 (1985).
[24] G. Galli, R. M. Martin, R. Car, and M. Parrinello, Phys. Rev. B **42**, 7470 (1990).
[25] P. C. Kelires, Phys. Rev. B **47**, 1829 (1993).
[26] D. W. Brenner, Phys. Rev. B **42**, 9458 (1990).
[27] C. Z. Wang, K. M. Ho, and C. T. Chan, Phys. Rev. Lett. **70**, 611 (1993).
[28] M. Menon and K. R. Subbaswamy, Phys. Rev. B **47**, 12754 (1993).
[29] Th. Köhler, Th. Frauenheim, D. Porezag, and D. A. Drabold (unpublished).
[30] J. Koike, D. M. Parkin, and T. E. Mitchell, Appl. Phys. Lett. **60**, 1450 (1992).
[31] U. Stephan and M. Haase, J. Phys.: Condens. Matter **5**, 9157 (1993).